JOURNAL OF THERMOPHYSICS AND HEAT TRANSFER
Vol. 24, No. 3, July–September 2010

Comprehensive Gas Ejector Model

Chaqing Liao
ABS Consulting, Irvine, California 92602
and
Frederick R. Best*
Texas A&M University, College Station, Texas 77843

DOI: 10.2514/1.46439

A comprehensive one-dimensional analytical model has been developed for gas ejector design and analysis. Unlike existing models, no assumptions have been made to simplify the momentum conservation equation for the ejector mixing chamber (that is, constant-pressure and constant-area models). Instead, the new model solves the momentum equation, which results in improved accuracy and versatility over existing models. Previous models can be derived from the new model as particular cases. These derivations provide new understanding of the relationships between the constant-pressure and constant-area one-dimensional ejector analytical models. The new model extends to the problems left unsolved by existing models and is efficient in analyzing off-design operating conditions, such as the shock that occurs in the primary stream. From the new model, the limitations on ejector design and operation are also recognized.

Nomenclature

A	=	area
D	=	temporary parameter
E	=	temporary parameter
h	=	enthalpy
κ	=	area ratio
M	=	Mach number
m	=	mass flow rate
P	=	pressure
R	=	gas constant
$\bar{R}$	=	universal gas constant
T	=	temperature
γ	=	specific heat ratio
Δs	=	entropy change
θ	=	area ratio
μ	=	pressure ratio
ρ	=	density
τ	=	pressure ratio
ω	=	entrainment ratio

Subscripts

a	=	flow station a
b	=	flow station b
e	=	exit
i	=	isentropic
m	=	ejector mixed flow
p	=	ejector primary stream
s	=	ejector secondary stream
t	=	nozzle throat
x	=	shock wave
0	=	stagnation condition
1	=	ejector section 1
2	=	ejector section 2
3	=	ejector section 3
4	=	ejector section 4
$*$	=	critical/choked point

Received 21 July 2009; revision received 3 November 2009; accepted for publication 6 November 2009.

*Department of Nuclear Engineering, Space Engineering Research Center.

I. Introduction

A GAS ejector is a device that uses the momentum and energy transfer from a high-velocity primary jet to induce a secondary fluid flow. Of particular interest to the authors are ejector applications in high-altitude aircraft and proton exchange membrane fuel cells [1,2].

The constant-pressure and constant-area models developed by Keenan and Neumann [3,4] are the basis of ejector design and performance analysis. Significant progress has been made for these widely used 1-D analytical models since 1950. A literature review carried out by Bonnington and King [5] cited more than 100 papers on gas ejectors. Another more recent and comprehensive review of published gas ejector research is given by Sun and Eames [6]. Among those relevant to the present work are Keenan and Neumann [3], DeFrate and Hoerl [7], Emanuel [8], Rice and Dandachi [9], Huang et al. [10], Huang and Chang [11], and Fabri and Siestrunck [12].

In an important literature review, Sun and Eames [6] stated that "advances have not been matched by the progress in constant-pressure mixing methods. . . and the question of the optimum shape of the mixing chamber has still not been answered. . . nobody has yet established a definite link between the performance of constant-area and constant-pressure ejectors."

Through this study, a comprehensive ejector model is developed that answers the previously mentioned open questions. Unlike the widely used constant-pressure and constant-area models, the new model does not require the assumption of either a constant-area mixing section or constant, uniform pressure in the mixing chamber. Both the constant-area and constant-pressure models can be derived from the new model as particular cases. An overexpansion or underexpansion shock usually occurs in either the supersonic diverging part of the primary nozzle or at the nozzle exit [13]. The existing models typically use coefficients obtained from experimental data for a particular ejector to correct for these losses [11,14].

This article is organized as follows: First, the new model derivation is presented and the gas ejector features from the perspective of the new model are discussed. Next, an example ejector is optimized for performance using the new model. Further, comparisons between the new model and the constant-pressure and constant-area models are performed. Finally, gas ejector operation and design limitations are analyzed using the new model.

II. Derivation of the New Ejector Model

The new model is developed for gas ejectors that have the general configuration shown in Fig. 1. The ejector is divided into four

sections: primary nozzle, mixing chamber, constant-area section, and subsonic diffuser. In practical applications, the subsonic diffuser may or may not be installed. If the area ratio of the mixing chamber entrance to mixing chamber exit is equal to unity, it becomes the constant-area mixing ejector.

The following assumptions are made for the new ejector model:

1) The inner wall of the ejector is adiabatic.

2) Friction loss is negligible.

3) The flow streams are uniform, 1-D, and in steady state.

4) Gases are in stagnation at the primary inlet and suction port.

5) The secondary inlet flow is not supersonic.

6) The primary and secondary streams have the same static pressure at the entrance of the mixing chamber (shown as cross section 1 in Fig. 1), i.e., $P_{p1} = P_{s1} = P_1$, where P_{p1} and P_{s1} are the static pressures of the primary and secondary stream at cross section 1 that are assumed to be a uniform pressure P_1.

7) The mixed flow is subsonic.

8) Both the primary and secondary streams can be considered ideal gases with constant specific heat ratios γ_p and γ_s.

The geometry of the primary nozzle determines the unique isentropic static pressure at the nozzle exit. In practical operation, a shock will occur due to underexpansion or overexpansion. The underexpansion shock usually occurs at the nozzle exit. The overexpansion shock may occur in the supersonic part of the nozzle or the nozzle exit, however, there is no way to determine the exact location of the shock. Separation may also take place if the shock occurs in the nozzle due to overexpansion. Because it is assumed that $P_{p1} = P_{s1} = P_1$, the parameter μ is used to relate P_1 with the secondary supply pressure P_{s0} as defined in Eq. (1)

$$\mu = \frac{P_1}{P_{s0}} \tag{1}$$

Further, Eq. (1) is related to the primary and secondary inlet pressures by Eq. (2)

$$P_{p1} = P_{s1} = P_1 = \mu P_{s0} \tag{2}$$

A. Mixing Chamber Entrance Flow Properties

Under the assumption that the secondary stream expands isentropically from the suction inlet to the mixing chamber entrance, the pressure ratio P_1/P_{s0} is related to the Mach number by Eq. (3)

$$\frac{P_1}{P_{s0}} = \mu = \left(1 + \frac{\gamma_s - 1}{2} M_{s1}^2\right)^{-\frac{\gamma_s}{\gamma_s - 1}} \tag{3}$$

In Eq. (3), γ_s is the specific heat ratio of the secondary gas, and M_{s1} is the Mach number of the secondary stream at the mixing chamber entrance. The above equation is rearranged to arrive at Eq. (4)

$$M_{s1}^2 = \frac{2}{\gamma_s - 1}\left(\mu^{-\frac{\gamma_s}{\gamma_s - 1}} - 1\right) \tag{4}$$

The expression for M_{s1} in Eq. (4) is substituted into the isentropic temperature function. The ratio of the secondary stream temperature at the mixing chamber entrance to its stagnation temperature T_{s1}/T_{s0} is expressed in Eq. (5)

$$\frac{T_{s1}}{T_{s0}} = \left(1 + \frac{\gamma_s - 1}{2} M_{s1}^2\right)^{-1} = \mu^{\frac{\gamma_s - 1}{\gamma_s}} \tag{5}$$

If the primary nozzle is operated at its design condition, the primary flow experiences isentropic expansion from the nozzle throat to the nozzle exit. The primary stream isentropic Mach number at the mixing chamber entrance M_{p1i} can be obtained by solving Eq. (6). The corresponding isentropic static pressureP_{p1i} is given by Eq. (7)

$$\frac{A_{p1}}{A_t} = \frac{1}{M_{p1i}} \sqrt{\left(\frac{1 + \frac{\gamma_p - 1}{2} M_{p1i}^2}{\frac{\gamma_p + 1}{2}}\right)^{\frac{\gamma_p + 1}{\gamma_p - 1}}} \tag{6}$$

$$\frac{P_{p1i}}{P_{p0}} = \left(1 + \frac{\gamma_p - 1}{2} M_{p1i}^2\right)^{-\frac{\gamma_p}{\gamma_p - 1}} \tag{7}$$

In Eqs. (6) and (7) A_{p1} and A_t are the nozzle exit and nozzle throat cross-sectional areas, γ_p is the primary stream gas specific heat ratio, and P_{p0} is the primary stream stagnation pressure.

If the nozzle is operated under off-design conditions, a shock will occur within the nozzle or at its exit. The subscript x is used to represent the flow properties after the shock. The primary stream static pressure and Mach number at the nozzle exit are $P_{p1} = P_1 = \mu P_{s0}$ and M_{p1}. For off-design operations $P_{p1} \neq P_{p1i}$, $M_{p1} \neq M_{p1i}$, and the total pressure will change, i.e., $P_{p0i} \neq P_{p0x}$, where P_{p0i} and P_{p0x} are the total pressures of the primary stream before and after the shock. Because it is an adiabatic process, the stagnation temperature does not change, $T_{p0i} = T_{p0x} = T_{p0}$. M_{p1} can be related to P_{p1} by mass conservation. The primary stream mass flow rate m_p is given by Eq. (8)

$$m_p = \frac{P_{p0} A_t}{\sqrt{T_{p0}}} \sqrt{\frac{\gamma_p}{R_p}\left(\frac{2}{\gamma_p + 1}\right)^{\frac{\gamma_p + 1}{\gamma_p - 1}}} \tag{8}$$

In Eq. (8), R_p is the primary stream gas constant. The mass flow rate can be expressed alternatively by Eq. (9)

$$m = \frac{PA}{(RT_0)^{1/2}} f_2(\gamma, M) \tag{9}$$

In Eq. (9), m is the mass flow rate, P is the local static pressure, A is the cross-sectional flow area, R is the gas constant, γ is the specific heat ratio, T_0 is the stagnation temperature, M is local Mach number, and the mass flow function $f_2(\gamma, M)$ is defined as Eq. (10)

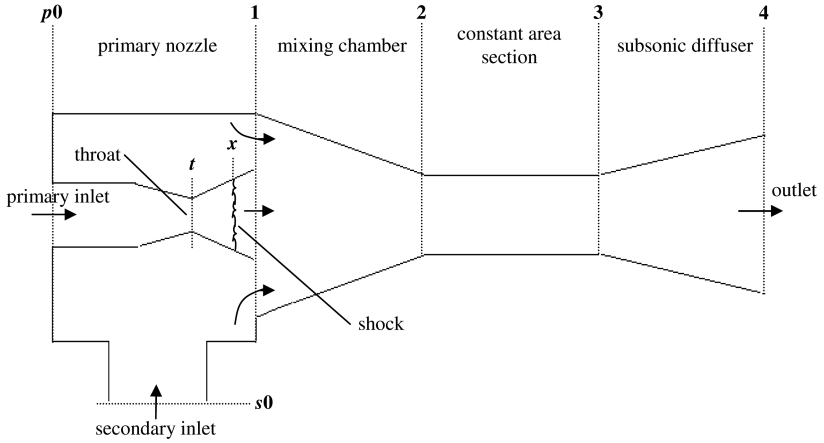

Fig. 1 Configuration of a general gas ejector.

$$f_2(\gamma, M) \equiv \frac{m}{PA}(RT_0)^{1/2} = M\left[\gamma\left(1+\frac{\gamma-1}{2}M^2\right)\right]^{1/2} \quad (10)$$

Combining Eqs. (8) and (9) yields Eq. (11)

$$\frac{P_{p1}A_{p1}}{(R_pT_{p0})^{1/2}} f_2(\gamma_p, M_{p1}^2) = \frac{P_{p0}A_t}{(R_pT_{p0})^{1/2}}\left[\gamma_p\left(\frac{2}{\gamma_p+1}\right)^{\frac{\gamma_p+1}{\gamma_p-1}}\right]^{1/2} \quad (11)$$

Substitute $P_{p1} = \mu P_{s0}$ into Eq. (11) and rearrange into Eq. (12)

$$f_2(\gamma_p, M_{p1}^2) = \frac{P_{p0}A_t}{\mu P_{s0}A_{p1}}\left[\gamma_p\left(\frac{2}{\gamma_p+1}\right)^{\frac{\gamma_p+1}{\gamma_p-1}}\right]^{1/2} \quad (12)$$

Equation (10) is then substituted into Eq. (12)

$$M_{p1}\left(1+\frac{\gamma_p-1}{2}M_{p1}^2\right)^{1/2} = \frac{P_{p0}A_t}{\mu P_{s0}A_{p1}}\left[\left(\frac{2}{\gamma_p+1}\right)^{\frac{\gamma_p+1}{\gamma_p-1}}\right]^{1/2} \quad (13)$$

Equation (13) is then rearranged into Eq. (14)

$$(\gamma_p-1)\mu^2M_{p1}^4 + 2\mu^2M_{p1}^4 - 2\left(\frac{P_{p0}A_t}{P_{s0}A_{p1}}\right)^2\left(\frac{2}{\gamma_p+1}\right)^{\frac{\gamma_p+1}{\gamma_p-1}} = 0 \quad (14)$$

The quadratic formula is then applied to Eq. (14)

$$M_{p1}^2 = \frac{-\mu + \sqrt{\mu^2 + 2(\gamma_p-1)(\frac{P_{p0}A_t}{P_{s0}A_{p1}})^2(\frac{2}{\gamma_p+1})^{\frac{\gamma_p+1}{\gamma_p-1}}}}{(\gamma_p-1)\mu} \quad (15)$$

The total pressure of the primary stream after the shock P_{p0x} can be derived from Eq. (3) and is shown in Eq. (16)

$$P_{p0x} = P_{p1}\left(1+\frac{\gamma_p-1}{2}M_{p1}^2\right)^{\frac{\gamma_p}{\gamma_p-1}} = \mu P_{s0}\left(1+\frac{\gamma_p-1}{2}M_{p1}^2\right)^{\frac{\gamma_p}{\gamma_p-1}} \quad (16)$$

The ratio of the total pressures before and after the shock is obtained

$$\frac{P_{p0i}}{P_{p0x}} = \frac{P_{p0}}{\mu P_{s0}(1+\frac{\gamma_p-1}{2}M_{p1}^2)^{\frac{\gamma_p}{\gamma_p-1}}} \quad (17)$$

B. Momentum Conservation Equation

The momentum conservation equation is applied to the mixing chamber as shown in Fig. 2. The momentum equation is then solved to find M_{m2}^2, the square of the Mach number at the mixing chamber exit. Equation (18) is the 1-D, x-direction momentum equation expressed in Mach numbers

$$P_{p1}A_{p1}(1+\gamma_pM_{p1}^2) + P_{s1}A_{s1}(1+\gamma_sM_{s1}^2) = P_{m2}A_{m2}(1+\gamma_mM_{m2}^2) \quad (18)$$

In Eq. (18), A_{m2}, P_{m2}, M_{m2}, and γ_m are the cross-sectional area, static pressure, Mach number, and specific heat ratio of the mixture at the mixing chamber exit (as shown in Fig. 2). Equation (18) is then rearranged into Eq. (19)

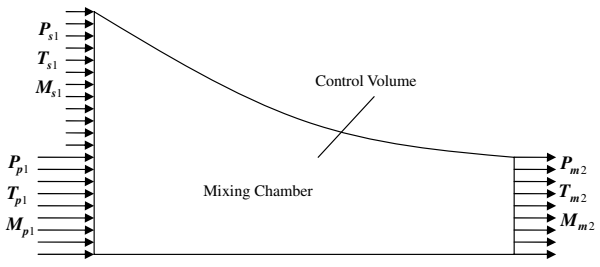

Fig. 2 Control volume of mixing chamber for comprehensive ejector model.

$$\frac{\mu P_{s0}A_{p1}}{P_{m2}A_{m2}}(1+\gamma_pM_{p1}^2) + \frac{\mu P_{s0}A_{s1}}{P_{m2}A_{m2}}(1+\gamma_sM_{s1}^2) = (1+\gamma_mM_{m2}^2) \quad (19)$$

Define the pressure ratio parameter τ

$$\tau \equiv \frac{P_{s0}}{P_{m2}} \quad (20)$$

The expression in Eq. (21) is derived by substituting Eqs. (1) and (20) into (19)

$$M_{m2}^2 = \frac{D\mu\tau - 1}{\gamma_m} \quad (21)$$

In Eq. (21), a grouping of terms D is defined in Eq. (22)

$$D = \frac{A_{p1}}{A_{m2}}(1+\gamma_pM_{p1}^2) + \frac{A_{s1}}{A_{m2}}(1+\gamma_sM_{s1}^2) \quad (22)$$

There are two unknown variables, μ and τ, in Eq. (21). It is desirable to express one of them as a function of the other. The mass flow rate at the mixing chamber exit is related to the secondary stream mass flow rate by Eq. (23)

$$\frac{m_m}{m_s} = \frac{1+\omega}{\omega} = \frac{P_{m2}A_{m2}}{P_{s1}A_{s1}}\frac{(R_sT_{s0})^{1/2}}{(R_mT_{m0})^{1/2}}\frac{f_2(\gamma_m, M_{m2})}{f_2(\gamma_s, M_{s1})} \quad (23)$$

In Eq. (23), the parameters m_m, R_m, and T_{m0} are the mass flow rate, gas constant, and stagnation temperature of the mixed stream, and ω is the entrainment ratio defined as the ratio of the secondary mass flow rate m_s to the primary mass flow rate m_p

$$\omega = \frac{m_s}{m_p} \quad (24)$$

According to the definitions of μ and τ, Eq. (25) is readily obtained from Eq. (23)

$$\frac{1+\omega}{\omega} = \frac{1}{\mu\tau}\frac{A_{m2}}{A_{s1}}\frac{(R_sT_{s0})^{1/2}}{(R_mT_{m0})^{1/2}}\frac{f_2(\gamma_m, M_{m2})}{f_2(\gamma_s, M_{s1})} \quad (25)$$

The expression of $f_2(\gamma_m, M_{m2})$ is substituted into Eq. (25) and rearranged

$$\frac{1+\omega}{\omega}\mu\tau = EM_{m2}\left[\gamma_m\left(1+\frac{\gamma_m-1}{2}M_{m2}^2\right)\right]^{1/2} \quad (26)$$

In Eq. (26), another grouping of terms E is defined in Eq. (27)

$$E = \frac{A_{m2}}{A_{s1}}\frac{(R_sT_{s0})^{1/2}}{(R_mT_{m0})^{1/2}}\frac{1}{f_2(\gamma_s, M_{s1})} \quad (27)$$

The expression for M_{m2} from Eq. (21) is substituted into Eq. (26)

$$\left[2\gamma_m\left(\frac{1+\omega}{\omega}\frac{\mu}{E}\right)^2 - (\gamma_m-1)D^2\mu^2\right]\tau^2 - 2D\mu\tau + (\gamma_m+1) = 0 \quad (28)$$

In Eq. (28), the variable τ has two solutions that correspond to the supersonic and subsonic mixed flow. In this study, the supersonic solution is discarded

$$\tau = \frac{D - \sqrt{D^2 - [2\gamma_m(\frac{1+\omega}{\omega}\frac{1}{E})^2 - (\gamma_m-1)D^2](\gamma_m+1)}}{2\gamma_m(\frac{1+\omega}{\omega}\frac{1}{E})^2\mu - (\gamma_m-1)D^2\mu} \quad (29)$$

Upon substitution of the expression for τ from Eq. (29) into Eq. (21), M_{m2}^2 takes the form of Eq. (30)

$$M_{m2}^2 = \frac{D}{\gamma_m}\frac{D - \sqrt{D^2 - [2\gamma_m(\frac{1+\omega}{\omega}\frac{1}{E})^2 - (\gamma_m - 1)D^2](\gamma_m + 1)}}{2\gamma_m(\frac{1+\omega}{\omega}\frac{1}{E})^2 - (\gamma_m - 1)D^2} - \frac{1}{\gamma_m} \tag{30}$$

The parameters P_1/P_{m2} and T_{m2}/T_{p1} can be expressed by Eqs. (31–33)

$$\frac{P_1}{P_{m2}} = \frac{P_1}{P_{s0}}\frac{P_{s0}}{P_{m2}} = \mu\tau \tag{31}$$

$$\frac{P_1}{P_{m2}} = \frac{D - \sqrt{D^2 - [2\gamma_m(\frac{1+\omega}{\omega}\frac{1}{E})^2 - (\gamma_m - 1)D^2](\gamma_m + 1)}}{2\gamma_m(\frac{1+\omega}{\omega}\frac{1}{E})^2 - (\gamma_m - 1)D^2} \tag{32}$$

$$\frac{T_{m2}}{T_{p1}} = \frac{T_{m0}}{T_{p0}}\frac{T_{p0}}{T_{p1}}\left(1 + \frac{\gamma_m - 1}{2}M_{m2}^2\right)^{-1} \tag{33}$$

In Eqs. (32) and (33), the specific heat ratio of the mixed flow γ_m is defined by Eq. (34)

$$\gamma_m = \frac{\frac{\gamma_p}{\gamma_p - 1} + \frac{\gamma_s}{\gamma_s - 1}\frac{R_s}{R_p}\omega}{\frac{1}{\gamma_p - 1} + \frac{1}{\gamma_s - 1}\frac{R_s}{R_p}\omega} \tag{34}$$

The stagnation temperature ratio of the mixed flow to the primary flow can be derived by applying energy conservation over the mixing chamber control volume

$$\frac{T_{m0}}{T_{p0}} = \frac{\frac{\gamma_p}{\gamma_p - 1} + \frac{\gamma_s}{\gamma_s - 1}\frac{R_s}{R_p}\frac{T_{s0}}{T_{p0}}\omega}{\frac{\gamma_p}{\gamma_p - 1} + \frac{\gamma_s}{\gamma_s - 1}\frac{R_s}{R_p}\omega} \tag{35}$$

C. Entrainment and Area Ratios

The mixing chamber geometry configuration can be represented by two area ratio parameters, κ and θ, which are defined in Eqs. (36) and (37)

$$\kappa \equiv \frac{A_{m2}}{A_t} \tag{36}$$

$$\theta \equiv \frac{A_1}{A_{m2}} \tag{37}$$

A further expansion of terms leads to Eqs. (38) and (39)

$$\frac{A_{m2}}{A_{p1}} = \kappa\frac{A_t}{A_{p1}} \tag{38}$$

$$\frac{A_{s1}}{A_{p1}} = \frac{A_t}{A_{p1}}\kappa\theta - 1 \tag{39}$$

According to its definition, the entrainment ratio ω is given by the following equation

$$\omega = \frac{m_s}{m_p} = \frac{\frac{P_{s1}A_{s1}}{(R_sT_{s0})^{1/2}}f_2(\gamma_s, M_{s1})}{\frac{P_{p1}A_{p1}}{(R_pT_{p0})^{1/2}}f_2(\gamma_p, M_{p1})} \tag{40}$$

Equation (40) can be simplified and rearranged into Eq. (41)

$$\omega = \frac{A_{s1}}{A_{p1}}\left(\frac{R_pT_{p0}}{R_sT_{s0}}\right)^{1/2}\frac{f_2(\gamma_s, M_{s1})}{f_2(\gamma_p, M_{p1})} \tag{41}$$

Substituting the expression for A_{s1}/A_{p1} into Eq. (41), ω is related to κ, θ, and the Mach numbers of each stream

$$\omega = \left(\frac{A_t}{A_{p1}}\kappa\theta - 1\right)\left(\frac{R_pT_{p0}}{R_sT_{s0}}\right)^{1/2}\frac{f_2(\gamma_s, M_{s1})}{f_2(\gamma_p, M_{p1})} \tag{42}$$

D. Entropy Change

The total entropy change Δs is a summation of the components of the entropy change due to the primary stream shock Δs_x and the entropy change due to the mixing of the two streams Δs_m

$$\Delta s = \Delta s_x + \Delta s_m \tag{43}$$

Equation (43) is then expanded

$$\Delta s = \frac{m_p(\Delta s|_p^{p1i\to p1} + \Delta s|_p^{p1\to m2}) + m_s\Delta s|_s^{s1\to m2}}{m_m} \tag{44}$$

In Eq. (44)

$$\Delta s|_p^{p1i\to p1}$$

is the primary stream entropy change due to the shock

$$\Delta s|_p^{p1\to m2}$$

is the primary stream entropy change due to the mixing process and

$$\Delta s|_s^{s1\to m2}$$

is the secondary stream entropy change due to the mixing process. Using mass conservation and the definition of ω, Eq. (44) can be rewritten as Eq. (45)

$$\Delta s = \frac{1}{1+\omega}\Delta s|_p^{p1i\to p1} + \frac{1}{1+\omega}\Delta s|_p^{p1\to m2} + \frac{\omega}{1+\omega}\Delta s|_s^{s1\to m2} \tag{45}$$

The entropy change of a stream experiencing a process change from state a to state b is defined by Eq. (46)

$$\Delta s|_{a\to b} = R\,\ell n\left[\frac{P_a}{P_b}\left(\frac{T_b}{T_a}\right)^{\frac{\gamma}{\gamma-1}}\right] \tag{46}$$

In Eq. (46), P_a, P_b, T_a, and T_b are the pressure and temperature at states a and b. Equation (46) is then applied to the primary stream

$$\Delta s|_p^{p1i\to p1} = R_p\,\ell n\left[\frac{P_{p1i}}{P_{p1}}\left(\frac{T_{p1}}{T_{p1i}}\right)^{\frac{\gamma_p}{\gamma_p-1}}\right] \tag{47}$$

Further expansion of Eq. (47) provides Eq. (48)

$$\Delta s|_p^{p1i\to p1} = R_p\,\ell n\left[\frac{P_{p0i}}{P_{p0x}}\left(\frac{T_{p0i}}{T_{p1i}}\right)^{-\frac{\gamma_p}{\gamma_p-1}}\left(\frac{T_{p0x}}{T_{p1}}\right)^{\frac{\gamma_p}{\gamma_p-1}}\left(\frac{T_{p1}}{T_{p1i}}\right)^{\frac{\gamma_p}{\gamma_p-1}}\right] \tag{48}$$

Because it is an adiabatic process, the stagnation temperature will not change

$$\Delta s|_p^{p1i\to p1} = R_p\,\ell n\left[\frac{P_{p0i}}{P_{p0x}}\right] \tag{49}$$

Substitution of Eq. (17) into Eq. (49) yields an expression for

$$\Delta s|_p^{p1i\to p1}$$

with respect to the variable μ and expressions for

$$\Delta s|_p^{p1\to m2}$$

and

$$\Delta s|_s^{s1\to m2}$$

$$\Delta s|_p^{p1i\to p1} = R_p\left[\ell n\left(\frac{P_{p0}}{P_{s0}}\right) + \ell n\left(\frac{1}{\mu}\right) - \frac{\gamma_p}{\gamma_p - 1}\ell n\left(1 + \frac{\gamma_p - 1}{2}M_{p1}^2\right)\right] \tag{50}$$

$$\Delta s|_p^{p1\to m2} = R_p\,\ell n\left[\frac{P_{p1}}{P_{m2}}\left(\frac{T_{m2}}{T_{p1}}\right)^{\frac{\gamma_p}{\gamma_p - 1}}\right] \tag{51}$$

$$\Delta s|_s^{s1\to m2} = R_s\,\ell n\left[\frac{P_{s1}}{P_{m2}}\left(\frac{T_{m2}}{T_{s1}}\right)^{\frac{\gamma_s}{\gamma_s - 1}}\right] \tag{52}$$

Considering $P_{p1} = P_{s1} = P_1$ and substitution of Eqs. (51) and (52) and into Eqs. (43) and (45), Δs_m is given by the following equation:

$$\Delta s_m = \frac{1}{1+\omega}\left\{(R_p + \omega R_s)\,\ell n\left(\frac{P_1}{P_{m2}}\right) + \omega R_s\frac{\gamma_s}{\gamma_s - 1}\ell n\left(\frac{T_{p1}}{T_{s1}}\right) + \left(R_p\frac{\gamma_p}{\gamma_p - 1} + \omega R_s\frac{\gamma_s}{\gamma_s - 1}\right)\ell n\left(\frac{T_{m2}}{T_{p1}}\right)\right\} \tag{53}$$

The term T_{p1}/T_{s1} is expanded as shown in Eq. (54)

$$\frac{T_{p1}}{T_{s1}} = \frac{T_{p1}}{T_{p0}}\frac{T_{p0}}{T_{s0}}\frac{T_{s0}}{T_{s1}} \tag{54}$$

In Eq. (54), the terms T_{p1}/T_{p0} and T_{s0}/T_{s1} are defined by Eqs. (55) and (56)

$$\frac{T_{p1}}{T_{p0}} = \left(1 + \frac{\gamma_p - 1}{2}M_{p1}^2\right)^{-1} \tag{55}$$

$$\frac{T_{s0}}{T_{s1}} = \left(1 + \frac{\gamma_s - 1}{2}M_{s1}^2\right) \tag{56}$$

III. Features of the Comprehensive Ejector Model

Entropy change is a function of the variable μ if the ejector geometry and boundary conditions are specified. The necessary geometric parameters are A_t and A_{p1}/A_t for the primary nozzle and κ and θ for the mixing chamber. The necessary boundary conditions are the primary and secondary fluid stagnation pressures and stagnation temperatures at the inlets. An example ejector is parameterized in Table 1, which will be used to demonstrate the new model. Air is supplied as the working fluid for both the primary and the secondary flows.

To investigate the features of the entropy change function $\Delta s = f(\mu)$, the total entropy change Δs and its two components Δs_x and Δs_m are plotted against μ in Fig. 3. The parameter μ should be in the range of $0 < \mu < 1$ for it to have physical meaning. It is observed that the Δs, Δs_x, and Δs_m curves change dramatically in the regions of very low μ(<0.15) and very high μ(>0.95). Obviously, a gas ejector would not be operated in these two regions. In the $\mu < 0.15$ region Δs_x is less than zero, which means the shock will not occur in this region. The entropy change curves are relatively flat in the region of $0.30 < \mu < 0.95$, which identifies the range of stable operation. Because the total entropy change is composed of the Δs_x and Δs_m components, the entropy change due to the mixing of the two streams or the separation of the primary stream may be included in the Δs_x term. Therefore, $\Delta s_m < 0$ is physically possible as long as the total entropy change Δs and its component Δs_x are positive.

Table 1 Geometry and operating parameters for an example gas ejector

A_t, m^2	A_{p1}/A_t	κ	θ	P_{p0}, psia	T_{p0}, K	P_{s0}, psia	T_{s0}, K
1.07e − 7	7.61	80	1.2	364.7	300	34.7	300

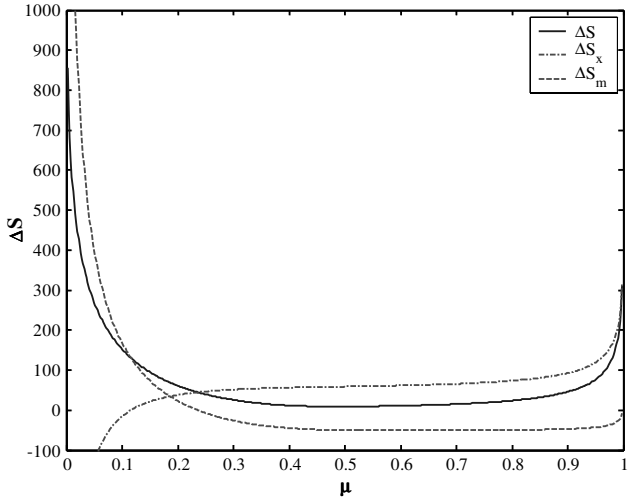

Fig. 3 Plots of the total entropy change and its two components.

Figure 4 is the plot of the entrainment ratio ω against μ. The entrainment ratio increases rapidly with increases in μ and will reach its maximum value at the point where $d\omega/d\mu = 0$. After reaching the maximum value, ω decreases. The location of the maximum ω should be different from the point of minimum total entropy change, because they are determined by different governing equations. However, the total entropy change curve in Fig. 3 and the entrainment ratio curve in Fig. 4 show that these two points are very close. In other words, the ejector has the best performance in terms of ω when it is operated in the region of the minimum total entropy change.

Entropy change is a measure of the irreversibility of a process. Mixing is a process in which the primary stream transfers part of its momentum to the secondary stream. Therefore, the irreversibility of the adiabatic mixing process results from the conversion of momentum to enthalpy. A large entropy change means large irreversibility; more momentum is converted to enthalpy. A small entropy change means less momentum is converted to enthalpy. In the region of the minimum entropy change, the conversion of momentum to enthalpy is minimal and the secondary stream gains the maximum momentum transfer from the primary stream. A higher secondary mass flow rate results when more momentum is provided for suction with a given fixed flow area, A_{s1}. This example demonstrates that the optimal ω is achieved when the total entropy change is at its minimum value.

As discussed previously, there are two solutions of τ that correspond to each μ value, one for supersonic and the other for

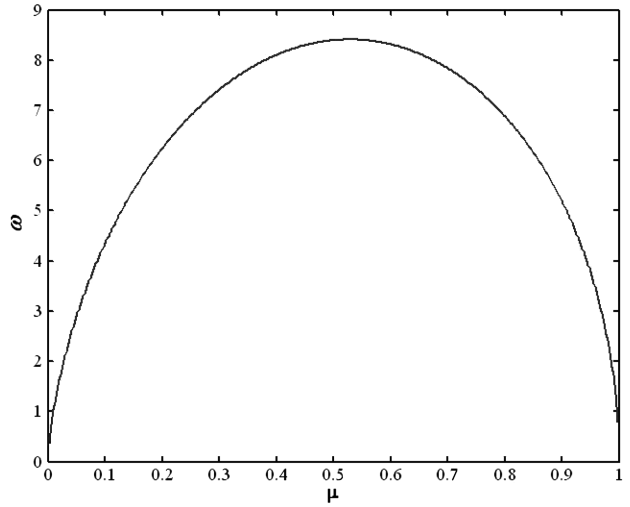

Fig. 4 Plot of entrainment ratio against μ.

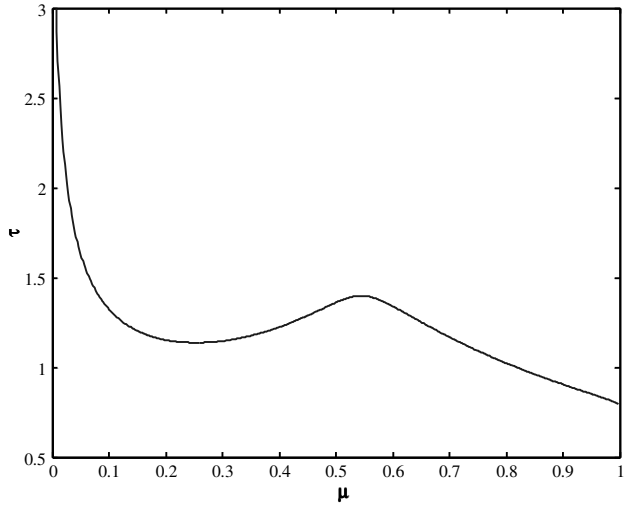

Fig. 5 Plots of τ against μ.

subsonic mixed flow (ejector downstream). In this research, the supersonic solution is discarded. The downstream flow can be supersonic if the ejector is used for an open system (such as rocket propulsion). In that scenario there will be entropy change at the ejector exit, which has not been included in our model.

Figure 5 shows the subsonic solution of τ vs μ. It is interesting to notice that in the regions of very low and very high μ, there is a one-to-one relationship between μ and τ. There could be two or even three values for μ for each τ in the region between the aforementioned two regions. Of course, it is not feasible to operate the gas ejector in the very low μ region because $\Delta s_x < 0$. Even so, it is possible for one τ to have two solutions of μ. Further analysis shows that one of these solutions corresponds to a supersonic secondary stream and the other corresponds to a subsonic secondary stream. In practical engineering, it is impossible to design an ejector with a supersonic secondary stream for a closed system.

IV. Optimal Ejector Performance

The optimal μ for the highest ω can be obtained by solving Eq. (42) at $\mathrm{d}\omega/\mathrm{d}\mu = 0$. If the operating domain $\mu \in (0, 1)$ is uniformly discretized, $\{\mu_1, \mu_2, \ldots, \mu_N\}$, with a cell size of $\Delta\mu$, then $d\omega/d\mu$ can be expressed in the discrete form given by Eq. (57)

$$\left.\frac{\mathrm{d}\omega}{\mathrm{d}\mu}\right|_{\mu_k+\frac{\Delta\mu}{2}} = \frac{\omega(\mu_{k+1}) - \omega(\mu_k)}{\Delta\mu} \tag{57}$$

The numerical solution of $\mathrm{d}\omega/\mathrm{d}\mu = 0$ is $\mu_{\mathrm{opt}} = \mu_I + \frac{\Delta\mu}{2}$ when Eq. (58) is true

$$\left.\frac{\mathrm{d}\omega}{\mathrm{d}\mu}\right|_{\mu_{\mathrm{opt}}} = \min\left(\left|\left.\frac{\mathrm{d}\omega}{\mathrm{d}\mu}\right|_{\mu_k+\frac{\Delta\mu}{2}}\right|\right) \tag{58}$$

To investigate the relationship between ω and the stream specific Mach numbers at the mixing chamber entrance, the parameters of normalized ω, M_{p1}, and M_{s1} are plotted in Fig. 6. M_{s1} intersects ω at the maximum ω value and $M_{s1} = 1$. This means that the ejector has the best performance when the secondary stream is choked at the mixing chamber entrance.

Using the numerical approach, $\mu_{\mathrm{opt}} = 0.529$ was found to be the solution of $\mathrm{d}\omega/\mathrm{d}\mu = 0$. Substituting the secondary flow properties (air in this case) and $M_{s1} = 1$ into Eq. (3), the calculation shows that choking occurs at $\mu_{\mathrm{choking}} = 0.528$. Considering the error due to numerical calculations, μ_{opt} is equal to μ_{choking}. This result is intuitively expected. The higher entrainment ratio means a higher secondary mass flow rate is induced. As is well known, the maximum mass flow rate is reached when the flow is choked.

V. Links Among Various Ejector Models

The Keenan constant-pressure mixing model assumes the static pressure in the mixing chamber to be uniform and constant, i.e., $P_{p1} = P_{s1} = P_{m2} = P_1$. In the comprehensive ejector model developed here, $P_{p1} = P_{s1} = P_1$ and P_1/P_{m2} are related to μ and τ by Eq. (31). The new model becomes the constant-pressure mixing model if the ejector is operated such that $P_1/P_{m2} = \mu\tau = 1$, i.e., $\tau = 1/\mu$. Should constant-pressure mixing exist, it will be located at the intersection point or the overlap between the curve of τ determined by Eq. (29) and the curve of $\tau = 1/\mu$.

To find the parameters of μ and τ for a constant-pressure mixing process, the τ curves for various θ at $\kappa = 200$ are plotted along with $\tau = 1/\mu$ in Fig. 7. The influence of parameter θ on τ is obvious: τ decreases as θ increases for a given μ. All τ curves are below the $\tau = 1/\mu$ curve. For $\theta = 1.0$, part of the τ curve in the high μ region ($\mu > 0.6$) is very close to the curve of $\tau = 1/\mu$, though they do not actually overlap and there is no intersection. For $\theta > 1.0$, the τ curves are further from the $\tau = 1/\mu$ curve. Therefore, a constant-pressure mixing operation is impossible. However, the assumptions made for the constant-pressure mixing model are valid for an ejector with small θ (close to 1.0). The constant-pressure model can predict ejector performance accurately under such conditions. If θ is large and far from $\theta = 1.0$, the assumptions made for the constant-pressure mixing model are invalid.

To investigate the influence of another geometric parameter κ, the τ curves for various κ at $\theta = 1.0$ are plotted along with $\tau = 1/\mu$ in Fig. 8. For $\kappa > 60$, the part of the τ curves in the high μ region ($\mu > 0.6$) are very close to the $\tau = 1/\mu$ curve and all curves are indistinguishable from each other. The τ curves for $\kappa < 60$ are distinguishable from the $\tau = 1/\mu$ curve.

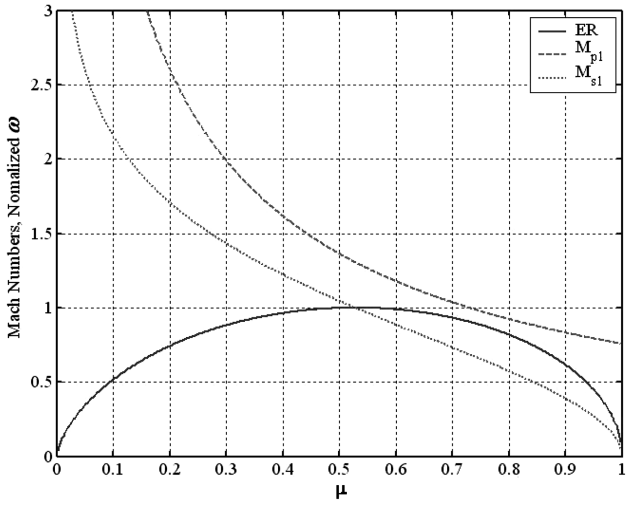

Fig. 6 Plots of M_{p1}, M_{s1}, and normalized ω.

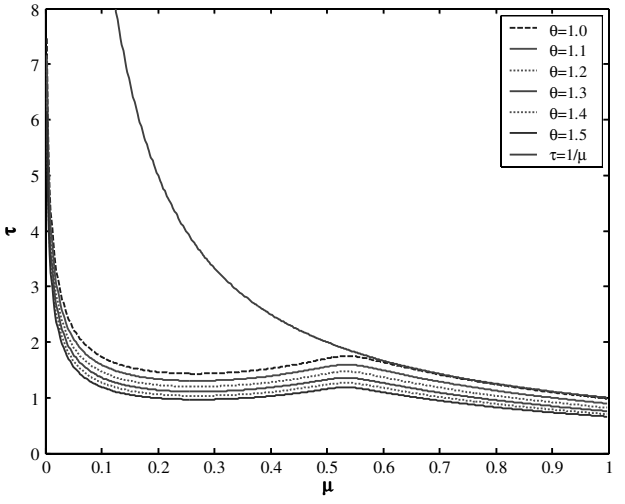

Fig. 7 Plots of τ against μ for various θ.

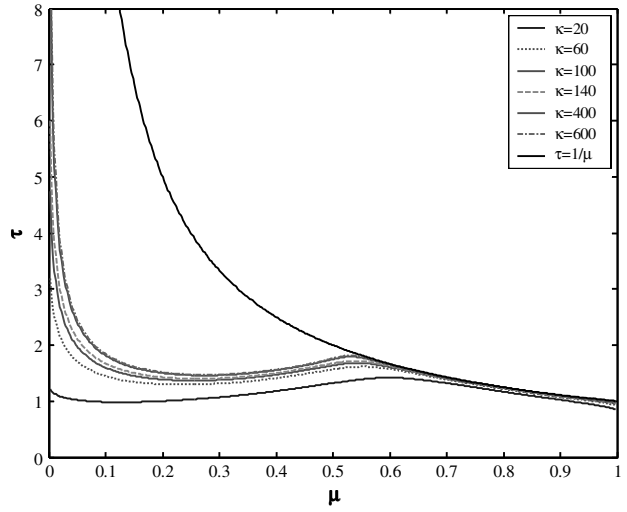

Fig. 8 Plots of τ against μ for various κ.

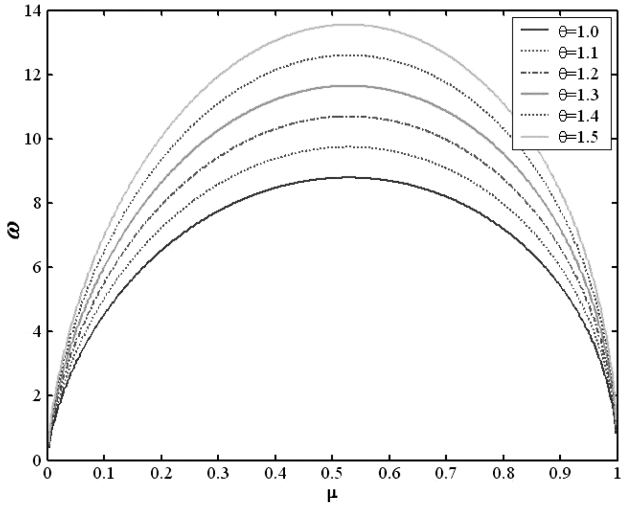

Fig. 9 Plots of ω against μ for various θ.

The ejector becomes a constant-area mixing ejector if $\theta = 1$. All the equations of the new model are valid for this particular case, though some could be further simplified. As a particular case, the constant-area ejector has all the generic features predicted for other ejectors, but also has its own special characteristics. From the standpoint of geometric configuration, unity is the lowest possible value of θ. It is observed from Fig. 9, that this particular ejector has the lowest entrainment. Actually, the constant-area mixing ejector gives the lowest performance, not only at the optimal point but also over the whole range of μ. This can be seen clearly in Fig. 9 where the plots of ω against μ for various θ are plotted at $\kappa = 100$.

The observations and discussions of Fig. 7 and 8 show that the assumptions made for a constant-pressure mixing ejector are accurate for $\theta = 1$. The constant-pressure model makes its most accurate predictions when the ejector has a constant-area mixing chamber. There is almost no difference between the predictions of the constant-pressure ejector model and constant-area ejector model when the area ratio is $\kappa > 60$. For a constant-area mixing ejector with a small area ratio ($\kappa < 20$), the predictions made by those two models may be significantly different.

VI. Limitations on Ejector Design and Operation

The new model can be used to design ejectors with specified operational requirements and conditions.

A. Design Limitations

In Fig. 10, the optimal ω surface (upper limit) for ejectors with various mixing chamber configurations is generated for the example case previously discussed and outlined in Table 1. Figure 10 shows that the upper limit of ω increases with an increase in parameters θ and κ. It is noticed that the upper limit of ω is lowest at $\theta = 1$ for a given κ.

In accordance with Fig. 10, the ejector should be designed with large θ and κ if high ω is desired. What are the limits for θ and κ? As discussed previously, ejectors fail to work if the total entropy change Δs is negative. Figure 11 is the surface plot of Δs for the ejectors parameterized by Table 1. A large part of this surface is below the plane of $\Delta s = 0$, which means that many ejectors cannot achieve the optimal ω values given by the surface in Fig. 10.

It is obvious that very limited geometric configurations could achieve the optimal entrainment ratio. An ejector could work at the optimal point only if it is designed with small κ or small θ. At $\theta = 1.0$, the κ can be as high as 1000 or even greater. When $\theta < 1.1$, the value of κ can be as high as 200. At $\theta = 1.2$, κ cannot be bigger than 100. From the standpoint of κ, the ejectors can achieve an optimal entrainment ratio even at $\theta = 2.0$ if κ is less than 10. However, the feasible θ value decreases very rapidly.

Constant-area mixing ejectors are of particular interest to designers because they are the most widely used ejector type. Figure 12 is the Δs surface plot for constant-area mixing ejectors with κ up to 1000. The total entropy change is positive across the operational range of μ as well as the investigated κ range. From this standpoint, the constant-area mixing ejector has the widest possible choice of geometry, though its performance is the worst.

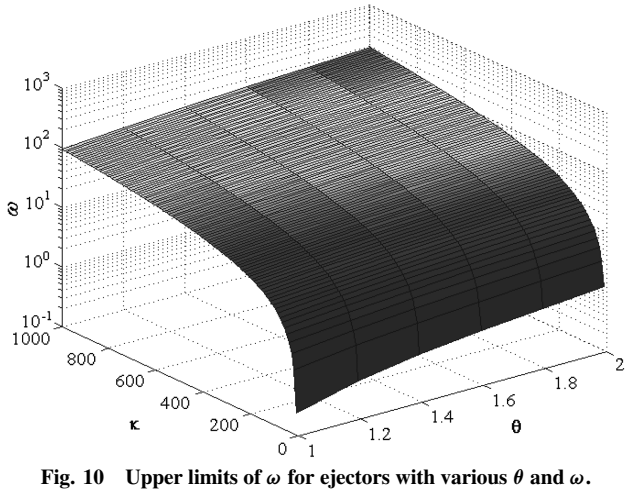

Fig. 10 Upper limits of ω for ejectors with various θ and ω.

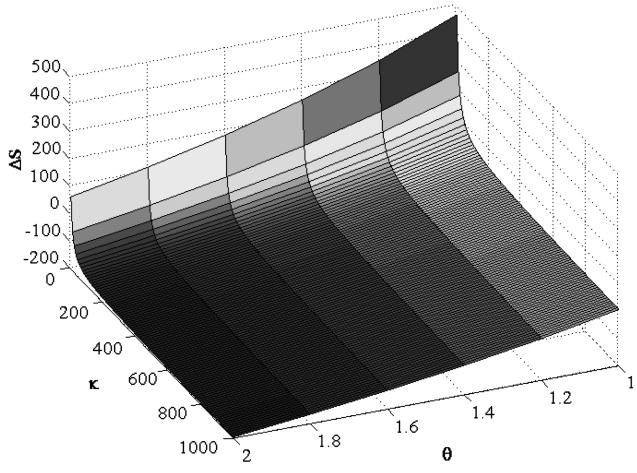

Fig. 11 Δs surface for ejectors with various θ and κ working at the optimal point.

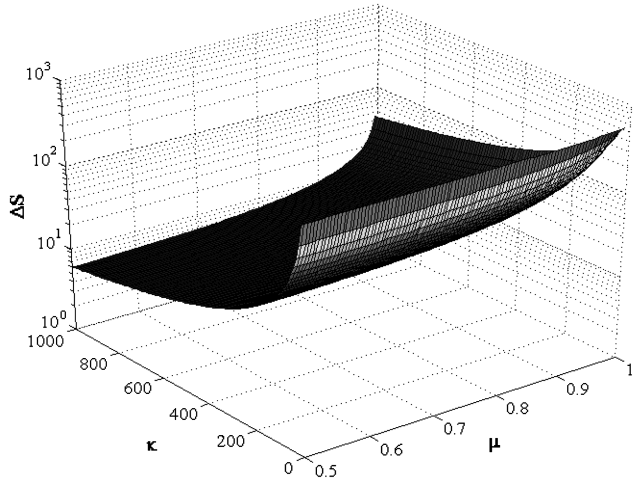

Fig. 12 Δs surface for constant-area mixing ejectors with various κ.

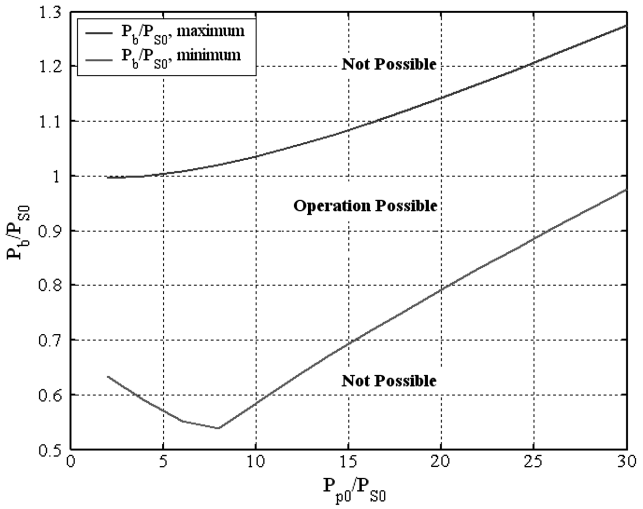

Fig. 13 Operational range of boundary pressure ratios.

B. Operational Limitations

In the new model, the two important operational parameters, μ and τ, are related to each other by Eq. (29). If one of them is given, the other can be calculated. It is more practical and convenient to specify the ejector outlet static pressure as a boundary condition, thus, τ is usually given.

The relationship between ejector performance and the boundary conditions is investigated, ie., the primary and secondary pressures at the inlets and the mixture pressure at the outlet. Performance curves are plotted against the pressure ratios P_{p0}/P_{s0} and P_b/P_{s0}, where P_b is the back pressure (or outlet static pressure for an ejector without a diffuser). To investigate the relationship between P_b/P_{s0} and P_{p0}/P_{s0}, both the maximum and minimum P_b/P_{s0} are plotted against P_{p0}/P_{s0} in Fig. 13. For a given P_{p0}/P_{s0}, the zone between the maximum P_b/P_{s0} curve and minimum P_b/P_{s0} curve is the operational area.

VII. Conclusions

A comprehensive analytical model for a gas ejector is developed. The widely used constant-pressure and constant-area models are shown to be two particular cases of the new model. Analysis shows that it is physically impossible to build an ejector with an exact constant-pressure mixing chamber. However, the predictions of the constant-pressure ejector model could be very accurate if the geometry of the ejector is close to the constant-area mixing ejector. If the mixing chamber is very different from constant-area mixing, a large error could result from the predictions of the constant-pressure model. The constant-area mixing ejector has the lowest performance, but has the widest operating range. Also, the constant-area ejector has the largest range of κ, the area ratio of the mixing chamber exit to primary nozzle throat.

Acknowledgments

This research was sponsored by the Department of Nuclear Engineering at Texas A&M University and by NASA Grant No. NNJ06HB52G. The authors would also like to express their appreciation to Adam M. Shephard, who has spent significant time editing this paper.

References

[1] Liao, C., "Gas Ejector Modeling for Design and Analysis," Ph.D. Dissertation, Nuclear Engineering Dept., Texas A&M Univ., College Station, TX, 2008.

[2] Lee, J. H., Sameen, A., Sanal Kumar, V. R., Kim, H. D., Choi, B. G., and Kim, K. H., "Studies on Ejector Systems for Hydrogen Fuel Cell," *Proceedings of 41st AIAA/ASME/SAE/ASEE Joint Propulsion Conference & Exhibit*, AIAA, Reston, VA, 2005.

[3] Keenan, J. H., and Neumann, E. P., "An Investigation of Ejector Design by Analysis and Experiment," *Journal of Applied Mechanics*, Vol. 72, 1950, pp. 299–309.

[4] Keenan, J. H., and Neumann, E. P., "A Simple Air Ejector," *Journal of Applied Mechanics*, Vol. 9, No. 2, 1942, pp. 75–81.

[5] Bonnington, S. T., and King, A. L., *Jet Pumps and Ejectors, A State of the Art Review and Bibliography*, 2nd ed., BHRA Fluid Engineering, Bedford, England, 1976.

[6] Sun, D. W., and Eames, I. W., "Recent Developments in the Design Theories and Applications of Ejectors: A Review," *Journal of the Institute of Energy*, Vol. 68, 1995, pp. 65–79.

[7] DeFrate, L. A., and Hoerl, A. E., "Optimum Design of Ejectors Using Digital Computers," *Chemical Engineering Progress Symposium Series*, Vol. 55, No. 21, 1959, pp. 43–51.

[8] Emanuel, G., "Optimum Performance for a Single-Stage Gaseous Ejector," *AIAA, Journal*, Vol. 14, No. 9, 1976, pp. 1292–1296.

[9] Rice, P., and Dandachi, J., "An Equation for the Prediction of Steam Flow Rate Required in the Design of Ejectors," *Transactions of the Institute of Chemical Engineering*, Vol. 69A, 1991, pp. 332–334.

[10] Huang, B. J., Chang, J. N., Wang, C. P., and Petrenko, V. A., "A 1-D Analysis of Ejector Performance," *International Journal of Refrigeration*, Vol. 22, No. 5, 1999, pp. 354–364. doi:10.1016/S0140-7007(99)00004-3

[11] Huang, B. J., and Chang, J. M., "Empirical Correlation for Ejector Design," *International Journal of Refrigeration*, Vol. 22, No. 5, 1999, pp. 379–388. doi:10.1016/S0140-7007(99)00002-X

[12] Fabri, J., and Siestrunck, R., "Supersonic Air Ejectors," *Advances in Applied Mechanics*, edited by Von Meiss and Von Karman, Academic Press, New York, 1958, pp. 1–34.

[13] Fox, R. W., McDonald, A. T., and Pritchard, P. J., *Introduction to Fluid Mechanics*, 6th ed., Wiley, Hoboken, NJ, 2003.

[14] Yapici, R., and Ersoy, H. K., "Performance Characteristics of the Ejector Refrigeration System Based on the Constant Area Ejector Flow Model," *Energy Conversion and Management*, Vol. 46, No. 18-19, 2005, pp. 3117–3135. doi:10.1016/j.enconman.2005.01.010